

**Supplementary Information**

**Highly Durable Fuel Cell Catalysts Using Crosslinkable Block Copolymer-Based Carbon Supports with Ultralow Pt Loadings**

*Juhyuk Choi<sup>†</sup>, Young Jun Lee<sup>†</sup>, Dongmin Park, Hojin Jeong, Sangyong Shin, Hongseok Yun, Jinkyu Lim, Junghun Han, Eun Ji Kim, Sun Seo Jeon, Yousung Jung, Hyunjoo Lee\*, and Bumjoon J. Kim\**

*Department of Chemical and Biomolecular Engineering, Korea Advanced Institute of Science and Technology (KAIST), Daejeon 34141, Republic of Korea*

\*E-mail: azhyun@kaist.ac.kr (H. L.)

\*E-mail: bumjoonkim@kaist.ac.kr (B. J. K.)

<sup>†</sup> Equally contributed

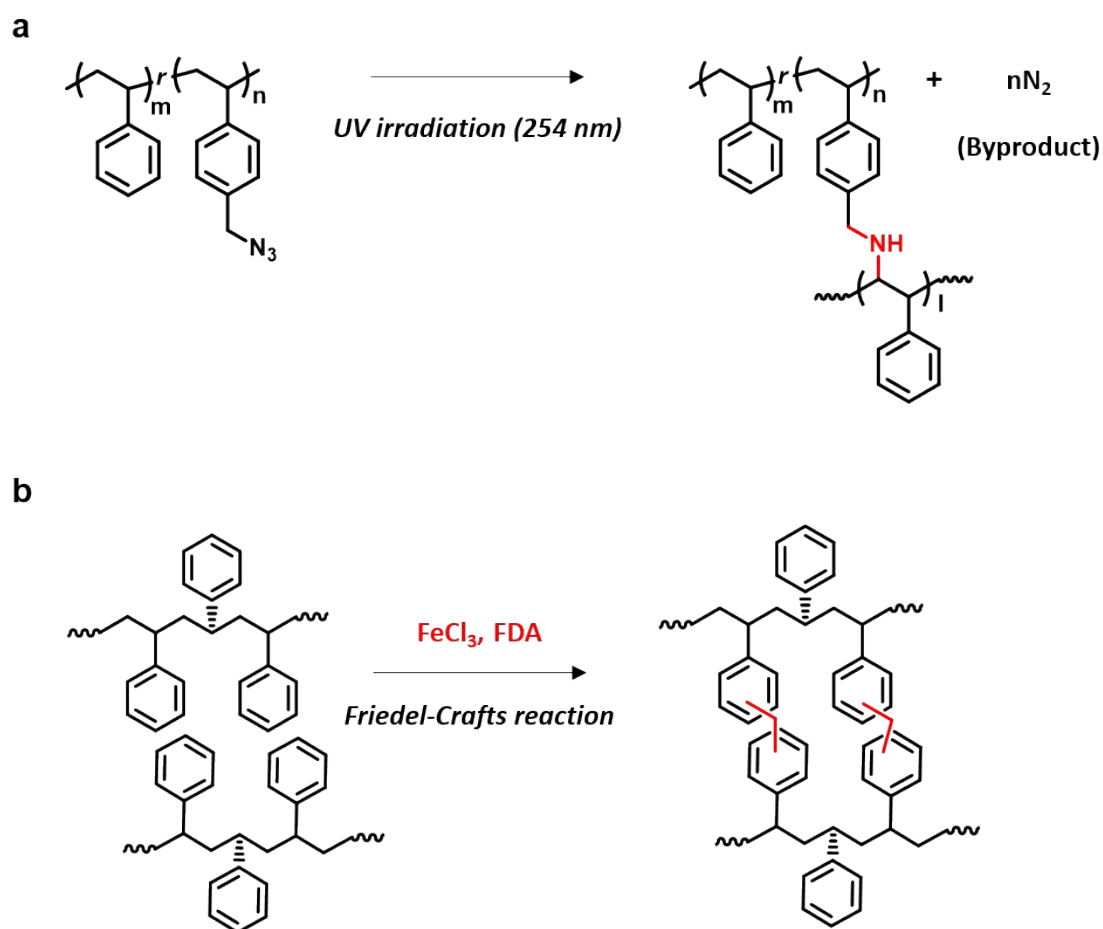


**Figure S1.** Schemes for **(a)** photo-crosslinking of P(S-*r*-N<sub>3</sub>) under ultraviolet light (254 nm) and **(b)** crosslinking using Friedel-Crafts reaction (FDA: formaldehyde dimethyl acetal).

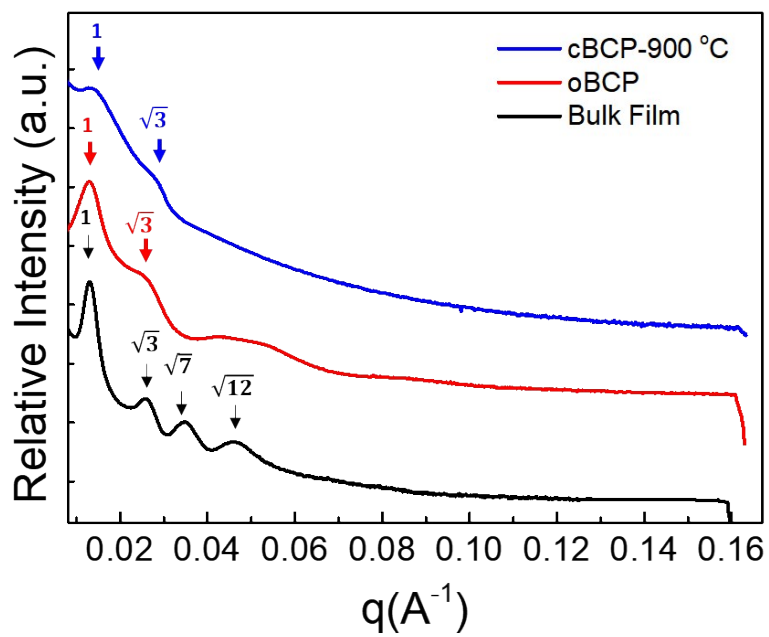


**Figure S2.** Small angle X-ray scattering (SAXS) data of bulk film of PS-*b*-PDMS containing P(S-*r*-N<sub>3</sub>), oBCP, and cBCP-900 °C.

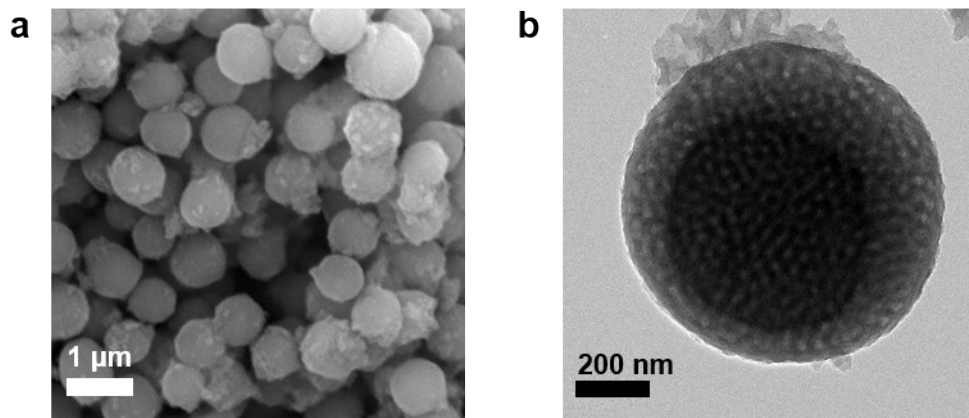


**Figure S3.** (a) SEM and (b) TEM images of mesoporous hyper-crosslinked BCP particles.

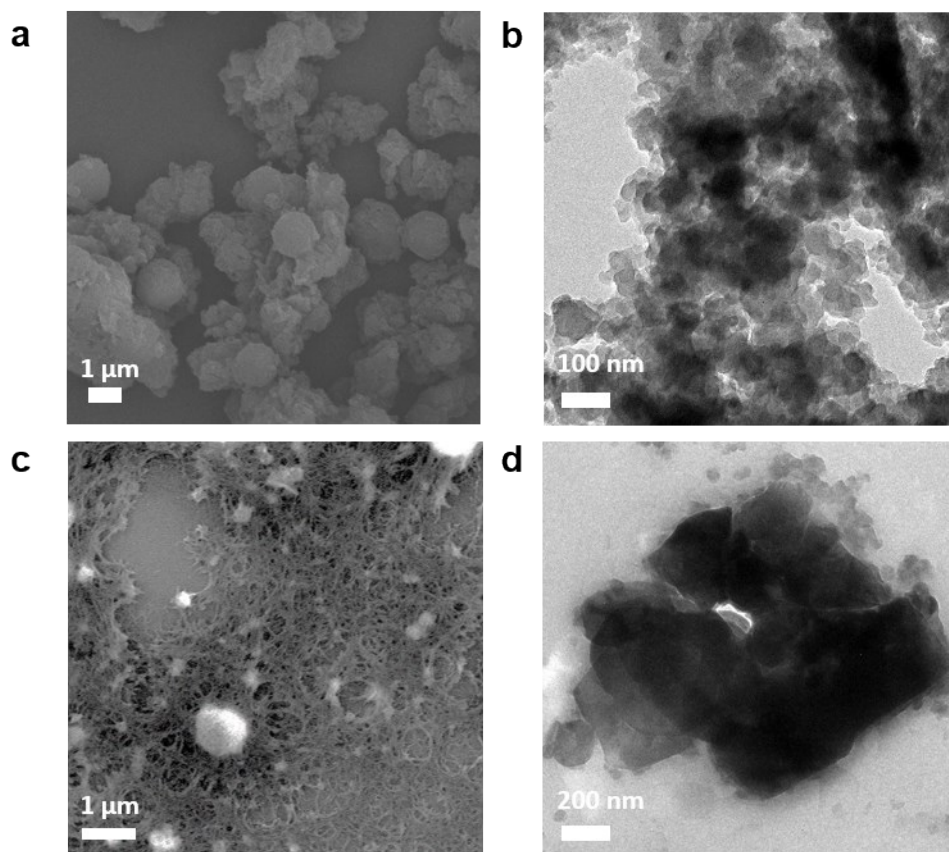


**Figure S4.** SEM and TEM images of **(a-b)** PS-*b*-PDMS particles prepared without P(S-*r*-N<sub>3</sub>) after Friedel-Crafts reaction and **(c-d)** PS-*b*-PDMS/P(S-*r*-N<sub>3</sub>) particles carbonized at 900 °C under N<sub>2</sub> gas flow without Friedel-Crafts reaction.

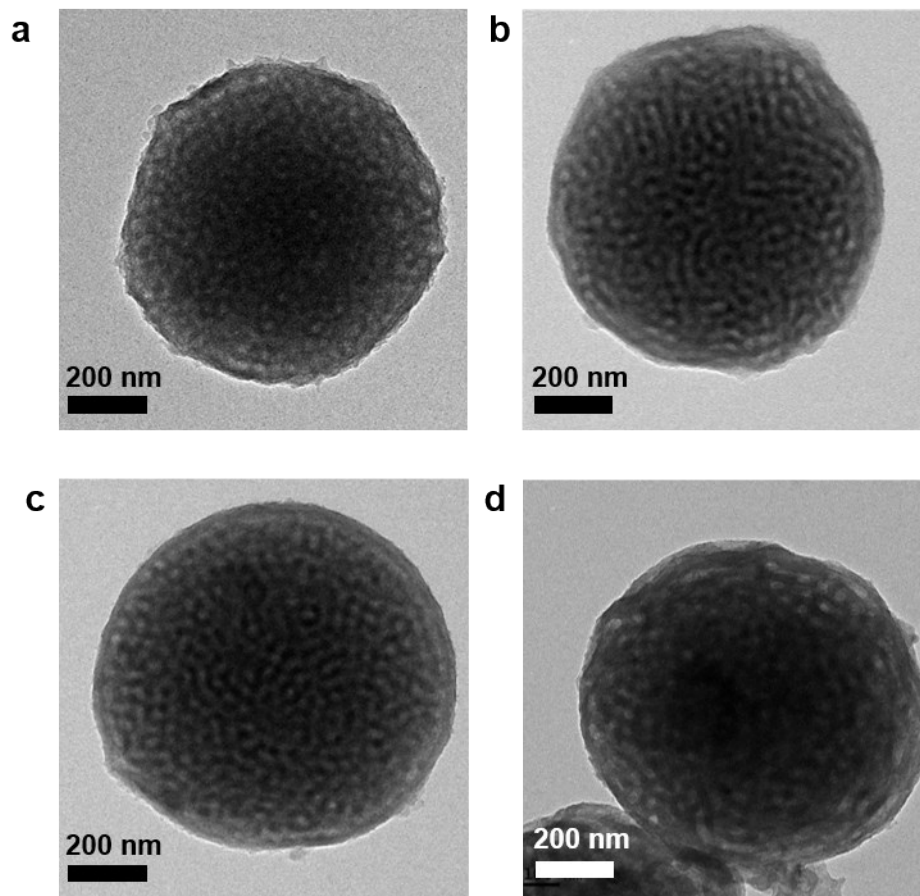


**Figure S5.** TEM images of cBCPs carbonized at (a) 700 °C, (b) 800 °C, (c) 900 °C, and (d) 1000 °C.

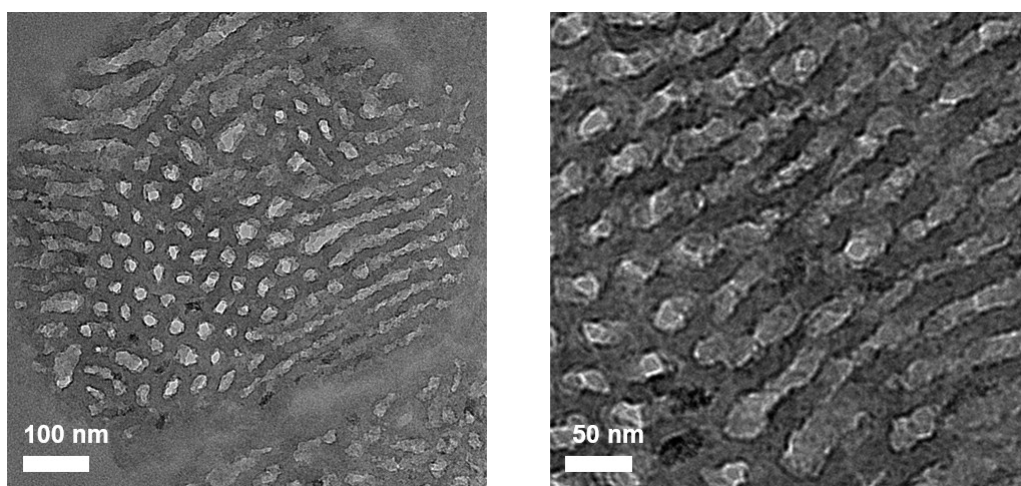


**Figure S6.** Cross-sectional TEM images of cBCP carbonized at 900 °C.

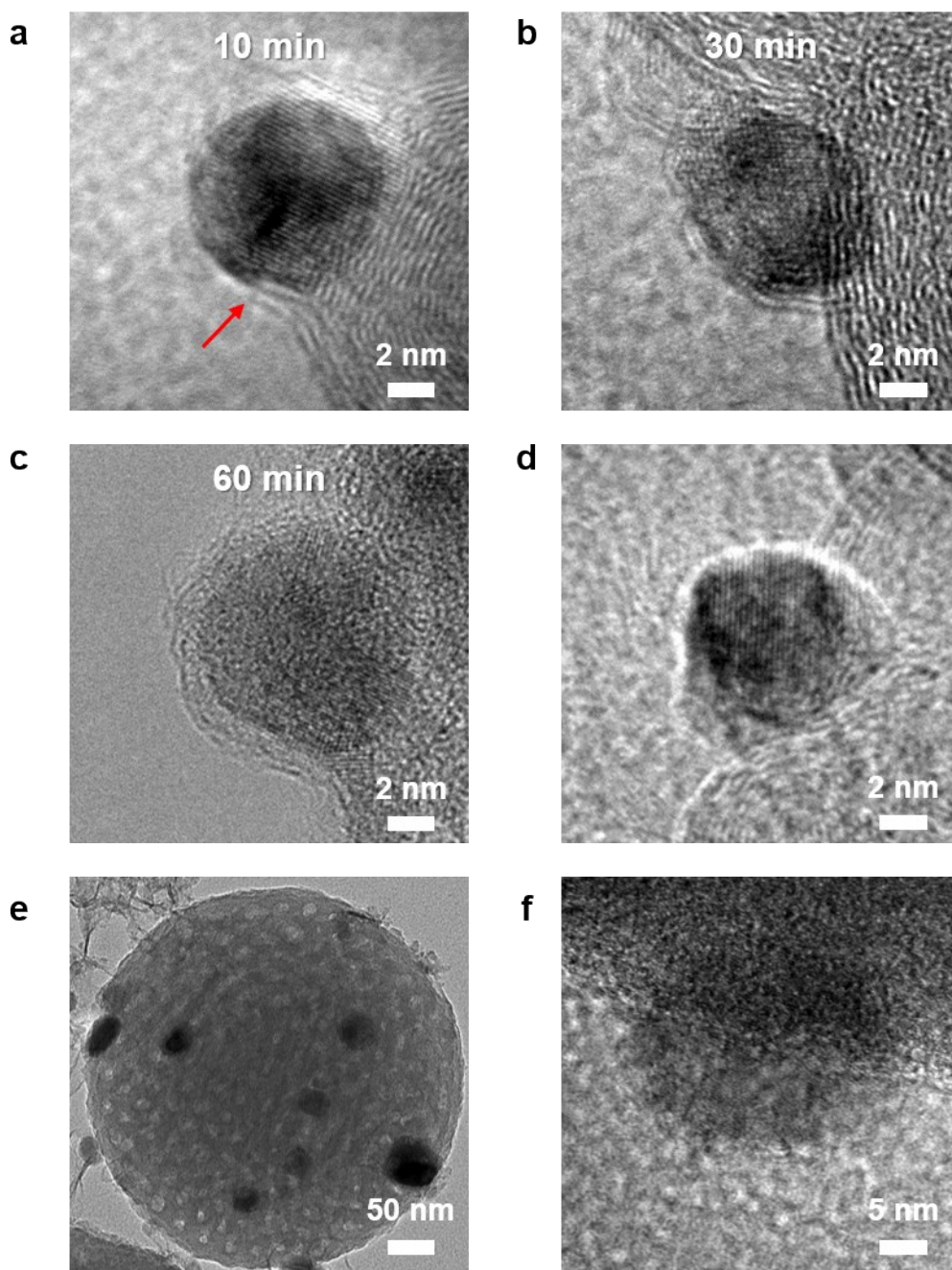


**Figure S7.** Formation of carbon shell. HR-TEM images of cBCP-PtFe catalyst after the reduction at 500 °C of **(a)** 10 min, **(b)** 30 min, **(c)** 60 min, **(d)** HR-TEM image of PtFe catalyst deposited on Vulcan carbon; the same synthesis procedure was used as the cBCP-PtFe carbonized at 900 °C except that Vulcan carbon was used instead of cBCP. **(e)** TEM and **(f)** HR-TEM images of cBCP-Fe catalyst prepared without Pt precursor using otherwise the same synthesis procedure.

**Table S1.** Elemental analysis results of hBCP, bare cBCP and cBCP-PtFe carbonized at 900 °C containing 1 wt% Pt.

	<b>hBCP (atomic %)</b>	<b>cBCP (atomic %)</b>	<b>cBCP-PtFe (atomic %)</b>
<b>C</b>	83.5	98.0	98.0
<b>H</b>	8.6	1.8	2.0
<b>N</b>	7.9	0.2	0

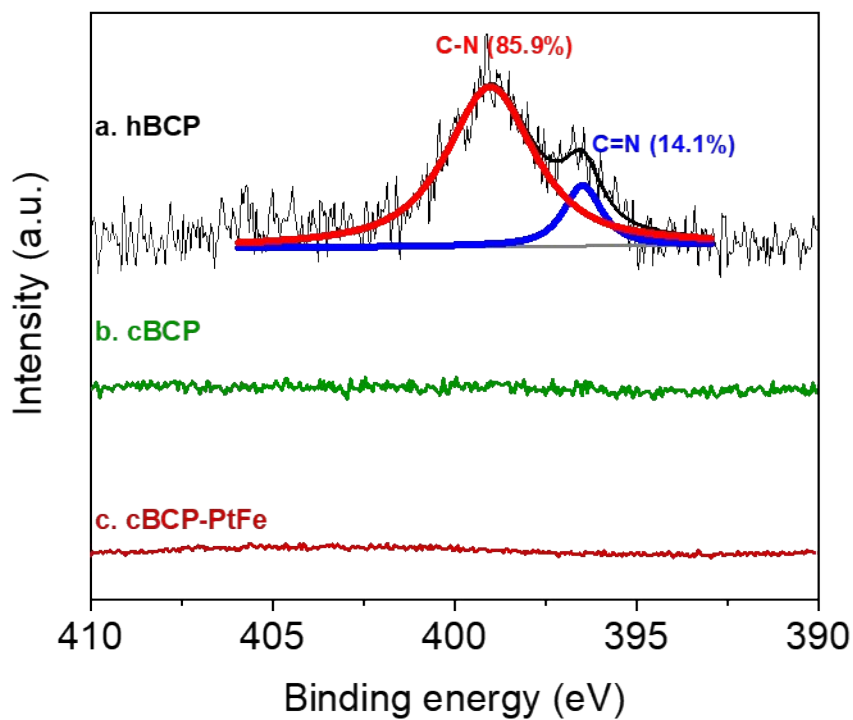


**Figure S8.** N 1s XPS results for (a) hBCP, and (b) bare cBCP carbonized at 900 °C. (c) N 1s HR-PES result for cBCP-PtFe carbonized at 900 °C containing 1 wt% Pt. XPS spectra were obtained at a fixed photon energy of 1486.7 eV using a monochromated Al K-alpha source. HR-PES spectrum was obtained at a photon energy of 650 eV using a synchrotron radiation source.

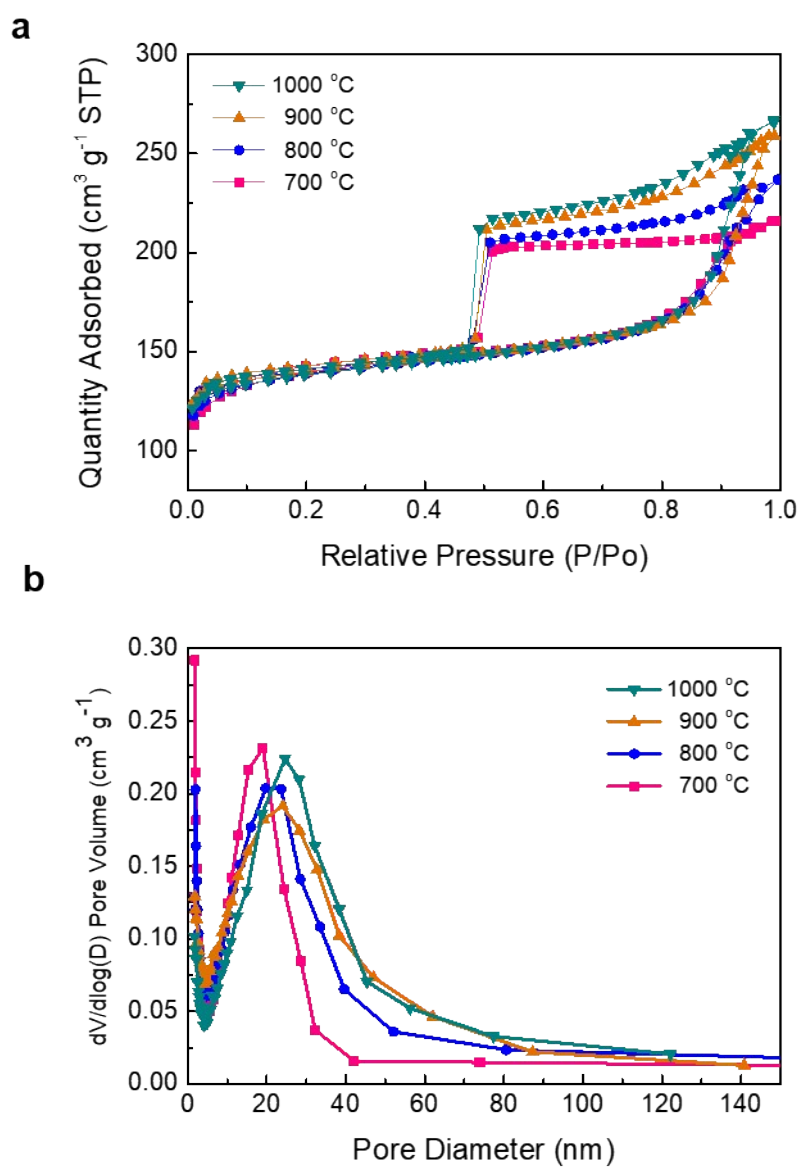


**Figure S9.** (a) BET  $\text{N}_2$  adsorption-desorption isotherms, and (b) pore size distribution.

**Table S2.** Textural property of cBCP-PtFe carbonized at various temperatures.

	<b>BET Surface Area (m<sup>2</sup> g<sup>-1</sup>)</b>	<b>Pore Volume (cm<sup>3</sup> g<sup>-1</sup>)</b>	<b>Pore Diameter (nm)</b>
<b>cBCP-PtFe-700°C</b>	488.5	0.33	20.1
<b>cBCP-PtFe-800°C</b>	508.9	0.35	22.4
<b>cBCP-PtFe-900°C</b>	567.7	0.38	24.1
<b>cBCP-PtFe-1000°C</b>	575.8	0.42	26.6

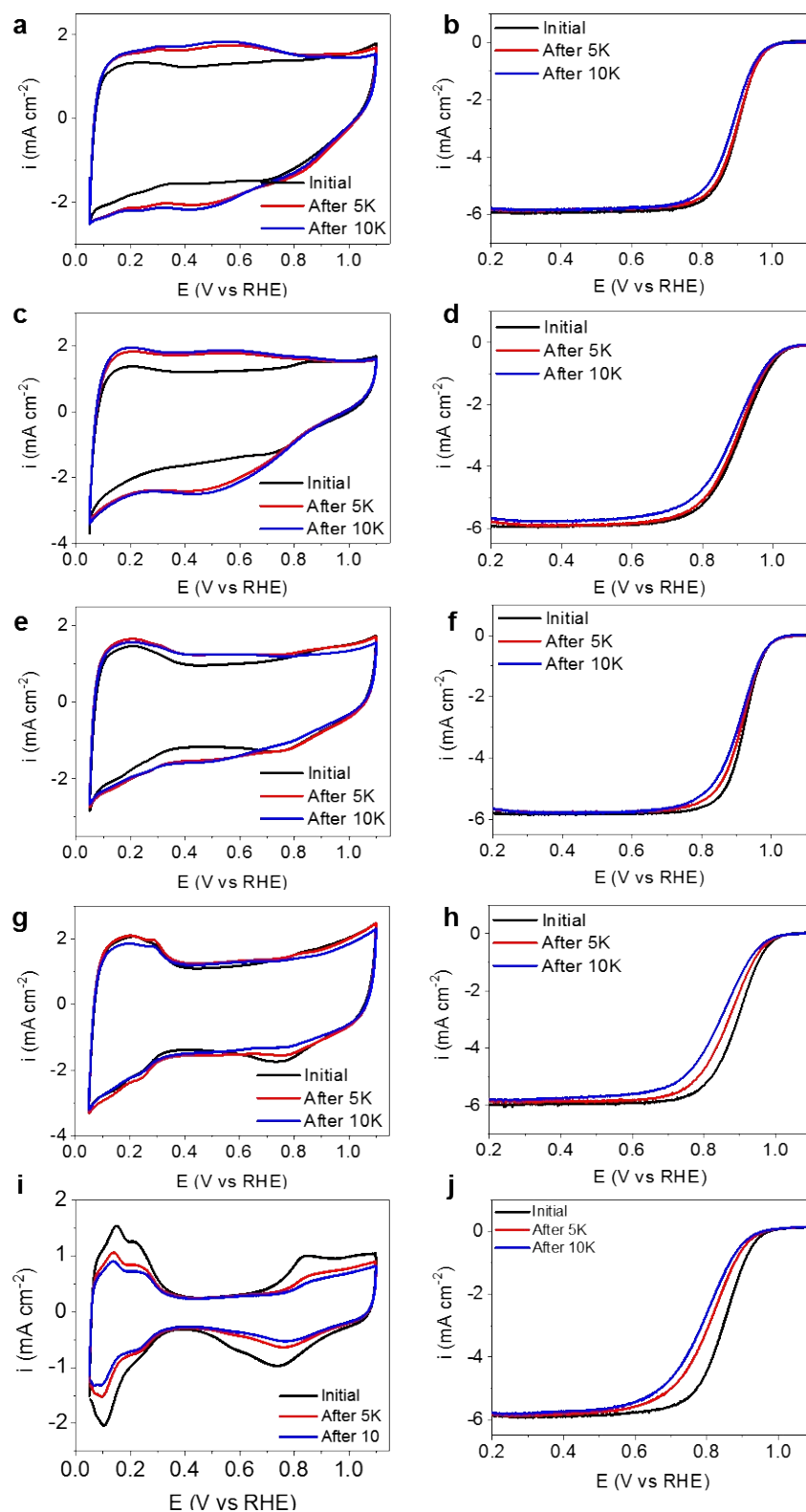


**Figure S10.** Cyclic voltammetry (CV) and linear sweep voltammetry (LSV) results of cBCP-PtFe with 1 wt% Pt carbonized at (a-b) 700 °C, (c-d) 800 °C, (e-f) 900 °C, (g-h) 1,000 °C, and (i-j) 20 wt% commercial Pt/C. CV and LSV results were obtained in Ar- and O<sub>2</sub>-saturated 0.1 M HClO<sub>4</sub> solution, respectively.

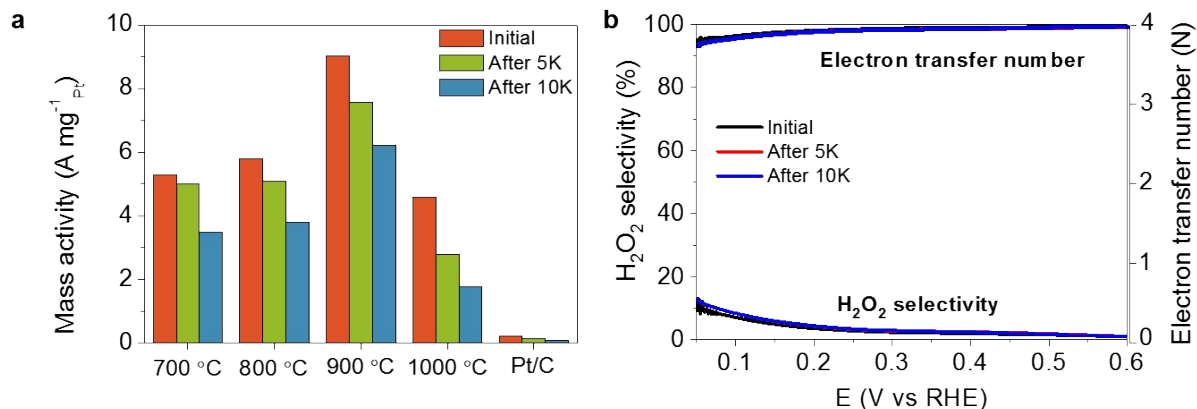


**Figure S11. (a)** ORR mass activities at 0.9 V<sub>RHE</sub> for cBCP-PtFe electrocatalysts with 1 wt% Pt and 20 wt% commercial Pt/C, and **(b)** H<sub>2</sub>O<sub>2</sub> selectivity and electron transfer number of the cBCP-PtFe carbonized at 900 °C. The ring currents for H<sub>2</sub>O<sub>2</sub> oxidation were measured by holding the Pt ring potential at 1.2 V during the ORR. The electron transfer number (n) and

$$H_2O_2 \text{ selectivity} \% = \frac{2I_r}{I_d + \frac{I_r}{N}} \times 100\%$$

$n = \frac{4I_d}{I_d + \frac{I_r}{N}}$  and

where  $I_d$  is the disk current,  $I_r$  is the ring disk, and  $N$  is the collection efficiency (0.37) of the working electrode.

**Table S3.** The concentrations of Fe ions leached after 10,000 cycles of ORR ADT in a half-cell for cBCP-PtFe carbonized at various temperatures.

	<b>700 °C</b>	<b>800 °C</b>	<b>900 °C</b>	<b>1000 °C</b>
<b>Leached Fe ion (ppb)</b>	2.35	2.54	2.12	3.24
<b>Fe retention (%)</b>	84.3	83.1	85.9	78.4

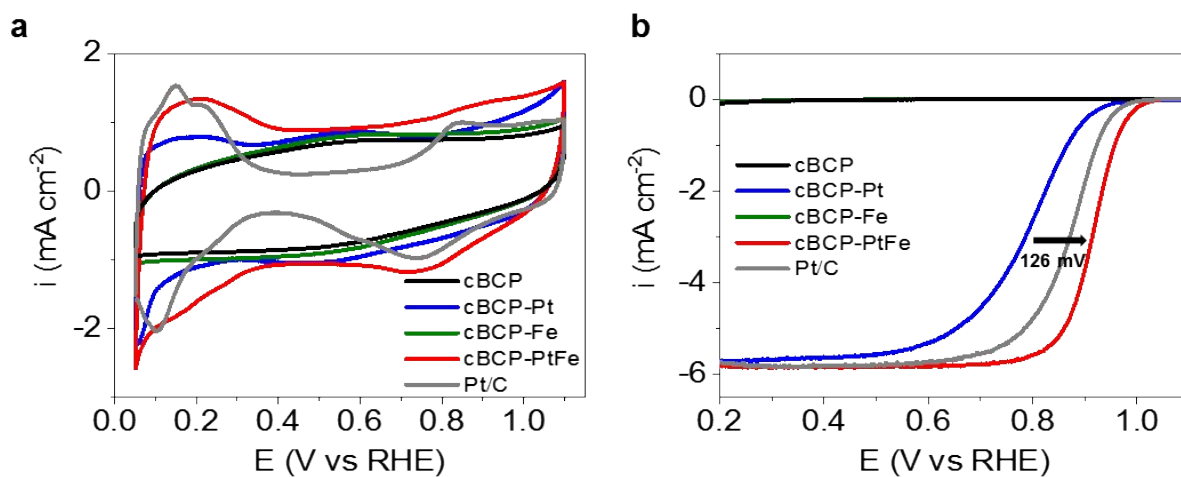


**Figure S12. (a)** CV and **(b)** LSV results of bare cBCP, cBCP-Pt, cBCP-Fe, and cBCP-PtFe, which were obtained with neither Pt nor Fe, with Pt only, with Fe only, and with both Pt and Fe, respectively. CV and LSV results were obtained in Ar- and O<sub>2</sub>-saturated 0.1 M HClO<sub>4</sub> solution, respectively.

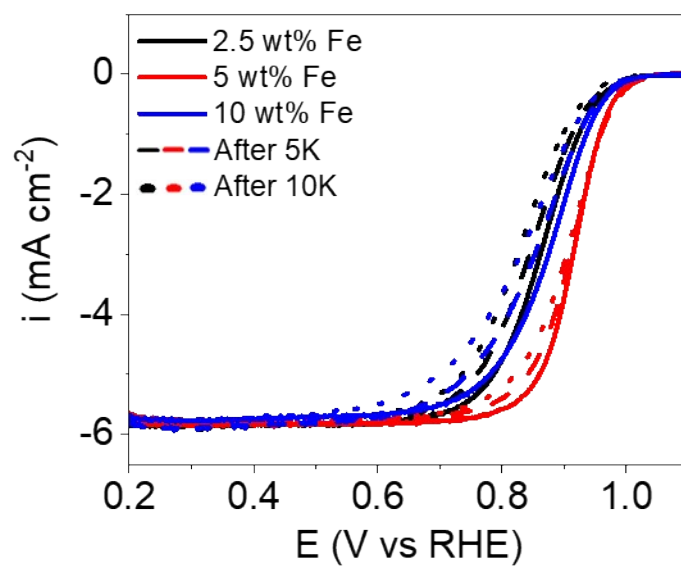


**Figure S13.** ORR polarization curves of cBCP-PtFe (900 °C) catalysts with various Fe contents. The durability test was performed by repeating CVs in 0.6-1.0 V<sub>RHE</sub>.

**Table S4.** Mass activity of the cBCP-PtFe (900 °C) catalysts with various Fe contents

	Mass activity (A mg <sup>-1</sup> )		
	Initial	After 5K	After 10K
2.5 wt% Fe	2.1	1.4	1.0
5 wt% Fe	9.0	7.6	6.2
10 wt% Fe	2.9	1.8	1.3

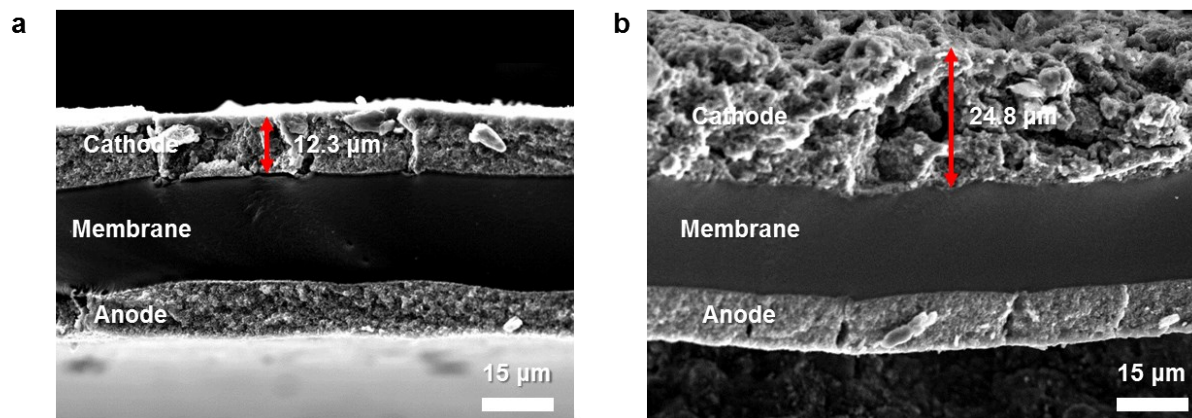


**Figure S14.** Cross-sectional SEM images of MEAs for **(a)** commercial Pt/C containing 20 wt% and **(b)** cBCP-PtFe containing 1 wt% Pt (carbonized at 900 °C).

**Table S5.** Pt loading required for the production of a kilowatt electricity.

	$g_{\text{Pt}} \text{ kW}^{-1}$	<b>Cathode Pt loading</b> ( $\text{mg}_{\text{Pt}} \text{ cm}^{-2}$ )	<b>Gas flow</b>	<b>Back pressure</b> (bar)	<b>Ref</b>
<b>cBCP-PtFe (900 °C)</b> <b>(This work)</b>	0.011	0.01	H <sub>2</sub> -O <sub>2</sub>	1.5	-
<b>LP@PF-1</b>	0.031	0.03	H <sub>2</sub> -O <sub>2</sub>	0.5	Science <b>362</b> , 1276-1281 (2018)
<b>LP@PF-2</b>	0.025	0.04	H <sub>2</sub> -O <sub>2</sub>	0.5	Science <b>362</b> , 1276-1281 (2018)
<b>Au-doped PtCo/C</b>	0.168	0.20	H <sub>2</sub> -O <sub>2</sub>	1.6	Appl. Catal. B:Environ, <b>247</b> , 142-149 (2019)
<b>NSTF-Pt<sub>3</sub>Ni<sub>7</sub></b>	0.143	0.10	H <sub>2</sub> -Air	0.5	J. Electrochem. Soc. <b>158</b> , B910-B918 (2011)
<b>P2-NA</b>	0.111	0.10	H <sub>2</sub> -Air	0.7	Energy Environ. Sci. <b>8</b> , 258-266 (2015)

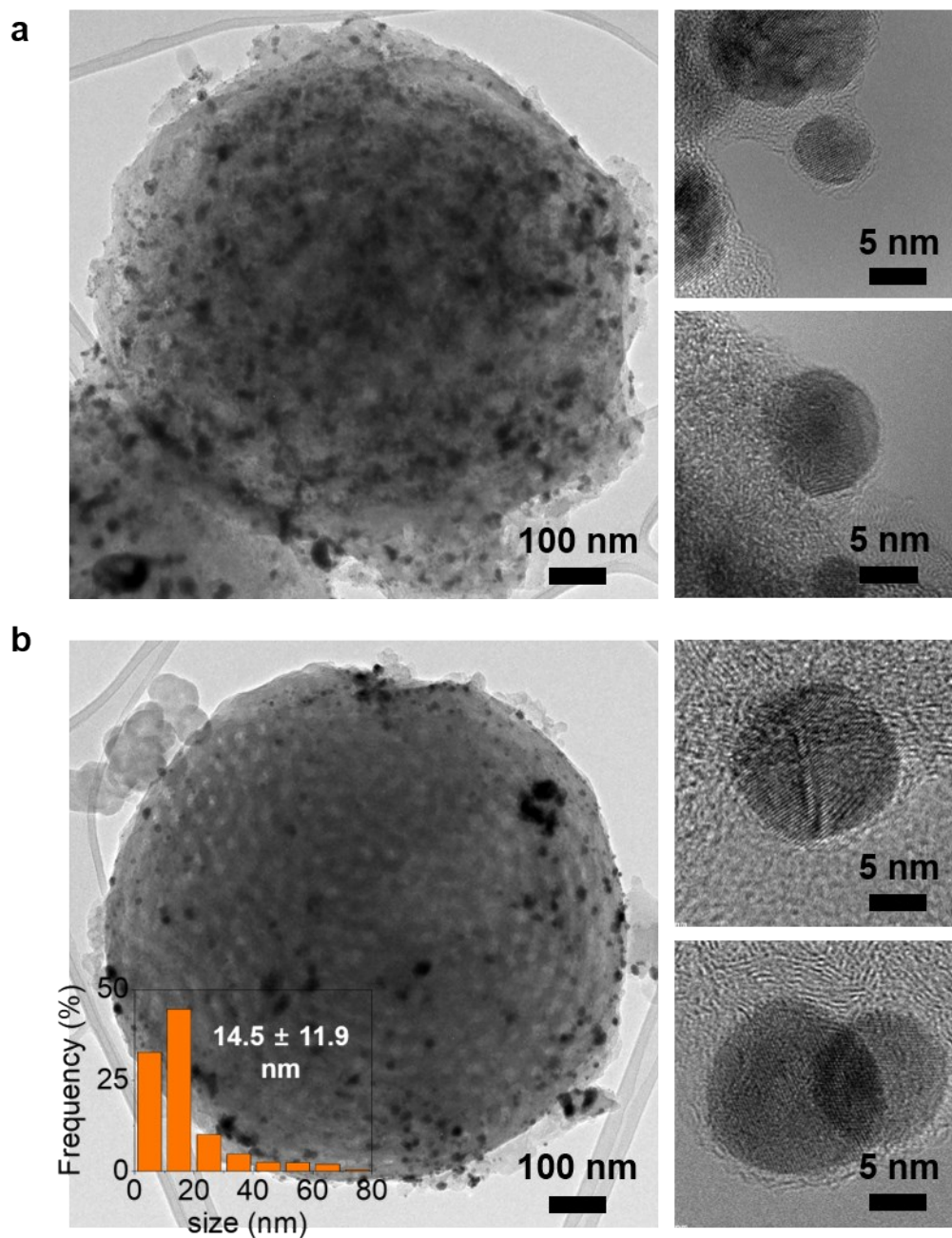


**Figure S15.** TEM images observed after the durability test **(a)** in a half-cell setup and **(b)** in a single-cell setup. The durability in a half-cell setup was tested by repeating the CV between  $0.6 V_{\text{RHE}}$  and  $1.0 V_{\text{RHE}}$  in  $\text{O}_2$ -saturated  $0.1 \text{ M HClO}_4$  solution for 10,000 cycles. The durability in a single cell setup was tested by repeating the CV between  $0.6 \text{ V}$  and  $1.0 \text{ V}$  with humidified  $\text{H}_2$  (200 sccm) to the anode and  $\text{N}_2$  (75 sccm) to the cathode for 30,000 cycles.

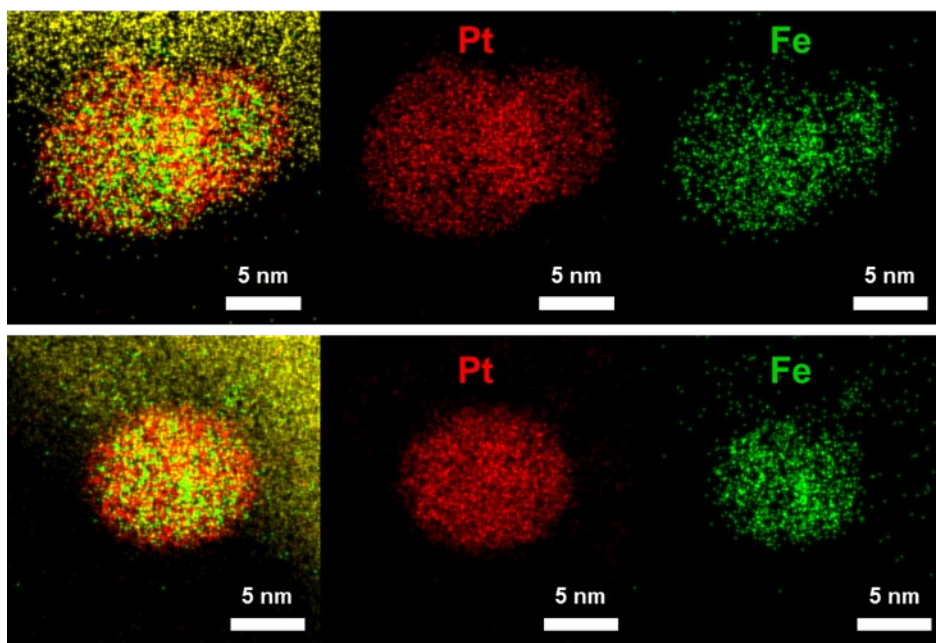


**Figure S16.** TEM-EDS mapping images of the cBCP-PtFe (900 °C) catalyst obtained after 30,000 cycles of the single cell durability tests.

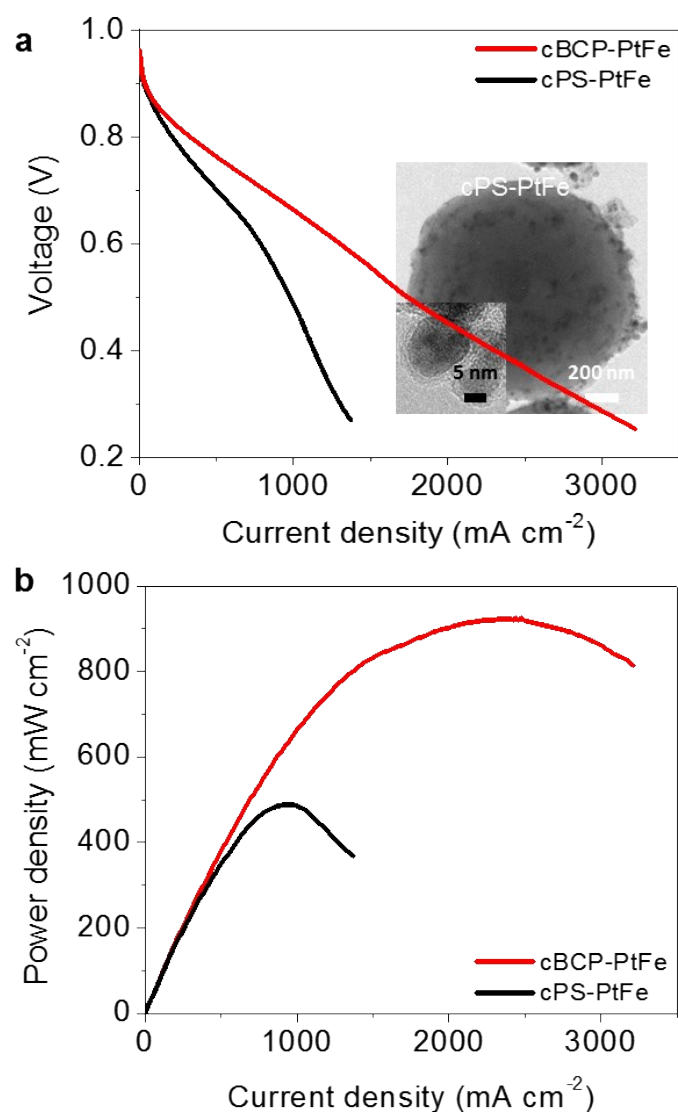


**Figure S17. (a)** i-V curves (inset: TEM image of a nonporous cPS-PtFe particle and HR-TEM image of carbon shell-capsulated PtFe particles located on the cPS-PtFe). **(b)** Power density curves in a single cell setup for cBCP-PtFe (porous particles) and cPS-PtFe (nonporous particles). Both samples contain 1 wt% Pt and were carbonized at 900 °C.

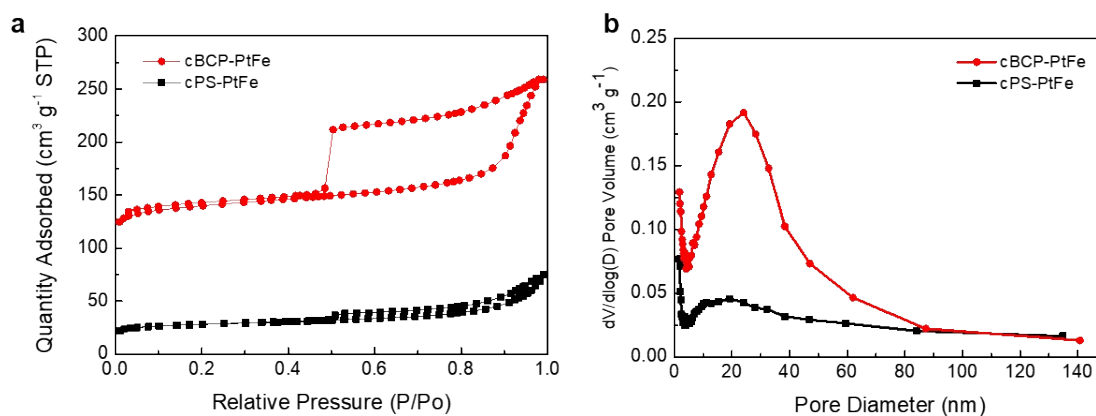


**Figure S18.** Textural property of the porous and nonporous particles. **(a)** BET N<sub>2</sub> adsorption-desorption isotherms, and **(b)** pores size distributions of the cBCP-PtFe and cPS-PtFe containing 1 wt% Pt. The carbonization was performed at 900 °C for both samples.

**Table S6.** Textural property of cBCP-PtFe and cPS-PtFe carbonized at 900 °C.

	<b>BET Surface Area (m<sup>2</sup> g<sup>-1</sup>)</b>	<b>Pore Volume (cm<sup>3</sup> g<sup>-1</sup>)</b>	<b>Pore Diameter (nm)</b>
<b>cBCP-PtFe</b>	567.7	0.38	24.1
<b>cPS-PtFe</b>	109.8	0.11	2.0

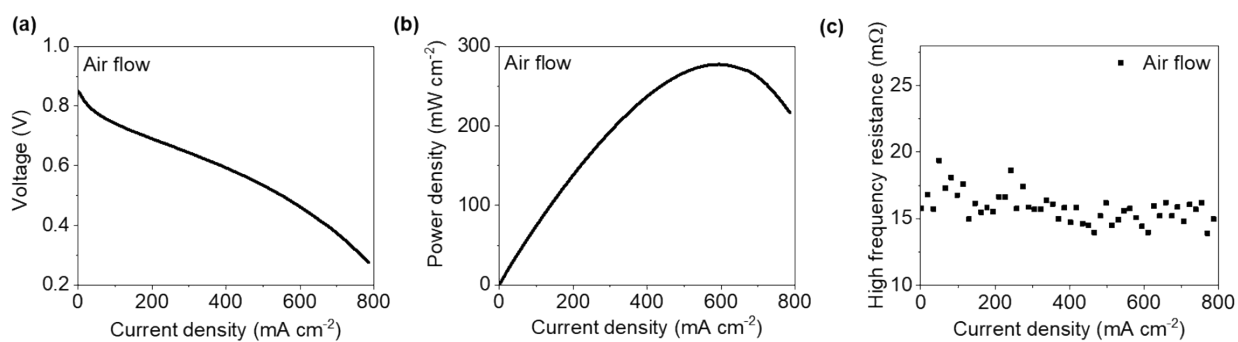


**Figure S19.** Single cell performance of cBCP-PtFe (900 °C) in H<sub>2</sub>-air flow condition; (a) i-V curve, (b) power density curve, and (c) high frequency resistance.

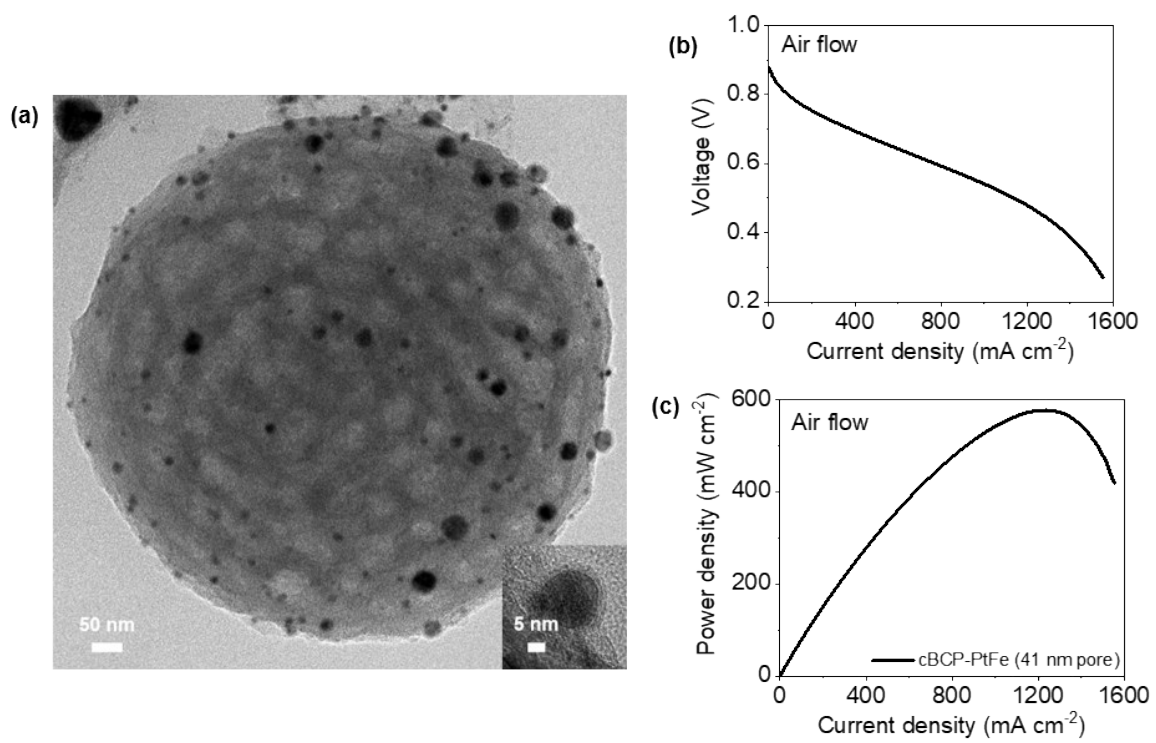


**Figure S20.** TEM image of cBCP-PtFe (900 °C) with 41 nm-sized pores, and its single cell performance in H<sub>2</sub>-air flow condition; (b) i-V curve, and (c) power density curve.

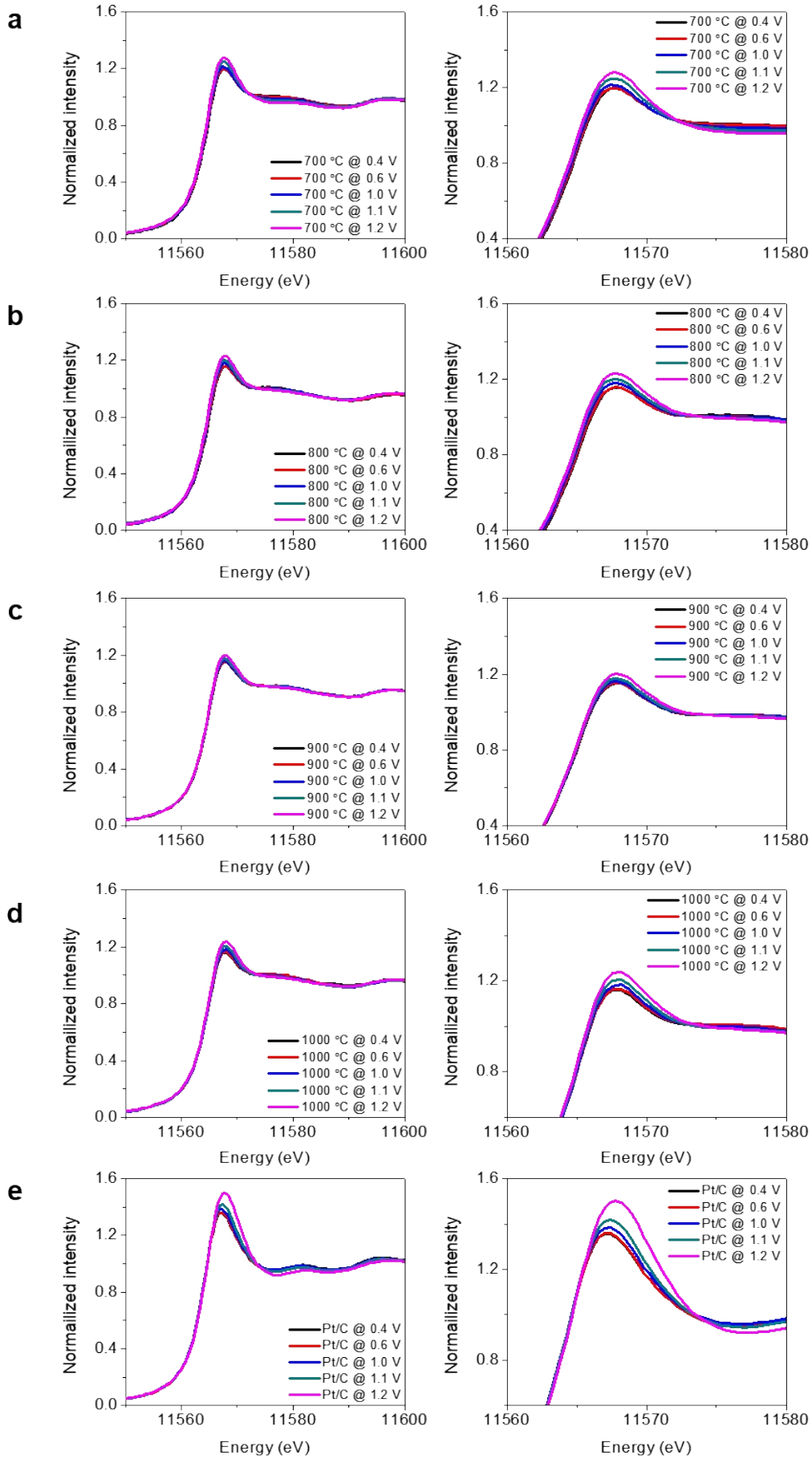


**Figure S21.** *In situ* XANES results of cBCP-PtFe with 1 wt% Pt carbonized at **(a)** 700 °C, **(b)** 800 °C, **(c)** 900 °C, **(d)** 1000 °C, and **(e)** commercial Pt/C with 20 wt% Pt. The XANES were measured by fluorescence mode using a home-made electrochemical cell when the potentials of 0.4, 0.6, 1.0, 1.1, 1.2 V<sub>RHE</sub> were applied. The working electrode was catalyst-coated carbon papers (39BC, SGL Carbon). Pt wire and Ag/AgCl electrode was used as counter electrode and reference electrode, respectively. Before acquiring the XAFS spectra, chronoamperometry was performed to obtain the stable current in each potential.

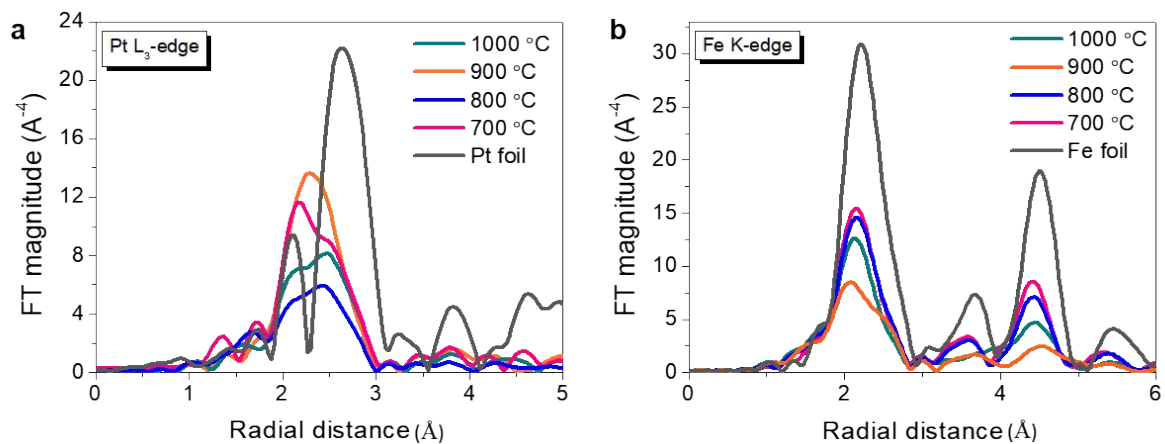


**Figure S22.** EXAFS results of cBCP-PtFe carbonized at various temperatures. **(a)** Pt L<sub>3</sub>-edge and **(b)** Fe-K edge  $k^3$ -weighted R-space FT-EXAFS spectra of the cBCP-PtFe electrocatalysts.

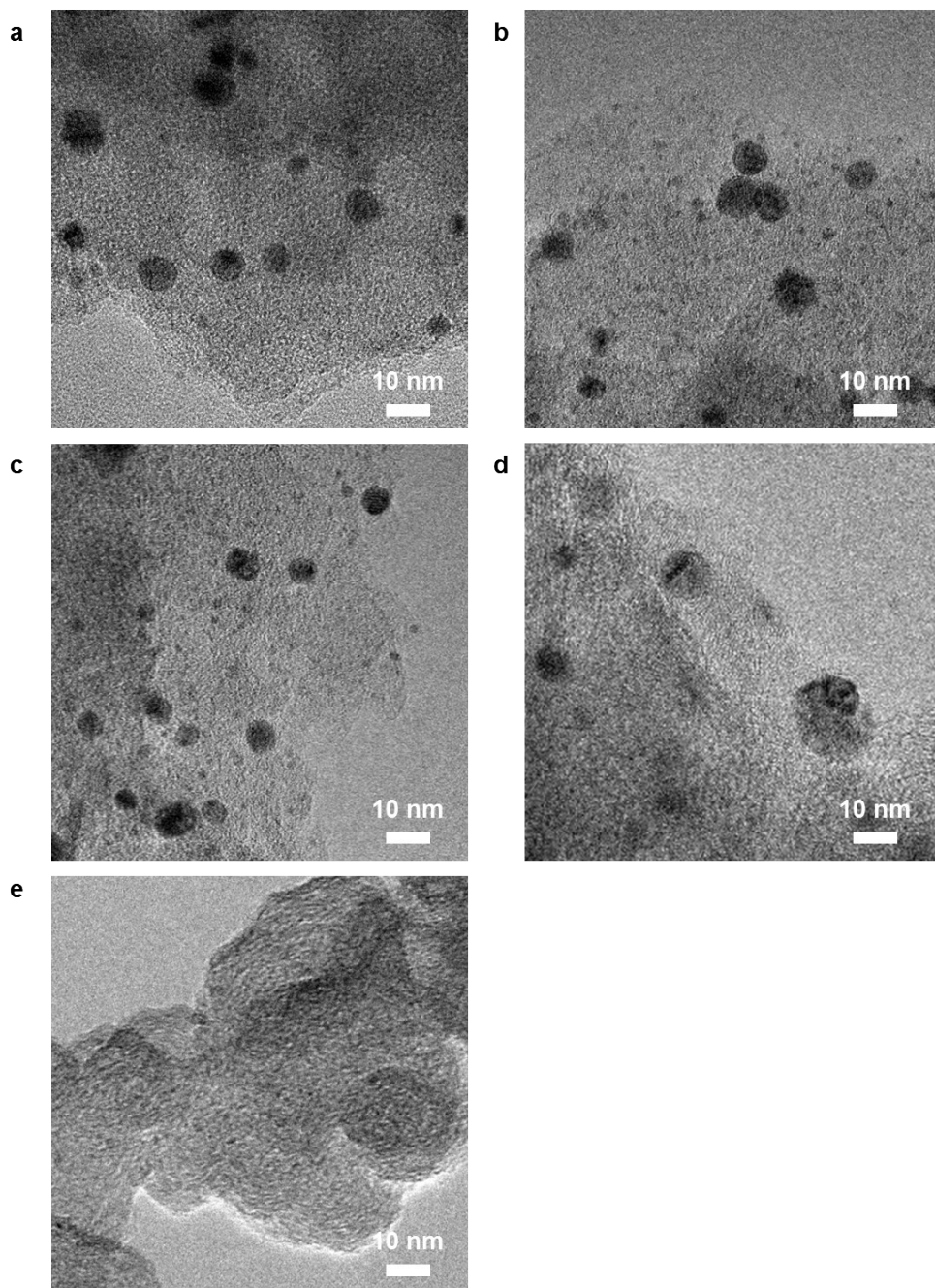


**Figure S23.** TEM images of cBCP-PtFe carbonized at **(a)** 700 °C, **(b)** 800 °C, **(c)** 900 °C, and **(d)** 1000 °C, in which all the samples contain 1 wt% Pt, after leaching. **(e)** TEM image of commercial Pt/C (20 wt% Pt) after leaching. The leaching treatment was performed with 0.1 M of aqua-regia solution under stirring (800 rpm) at 80 °C for 8 h.

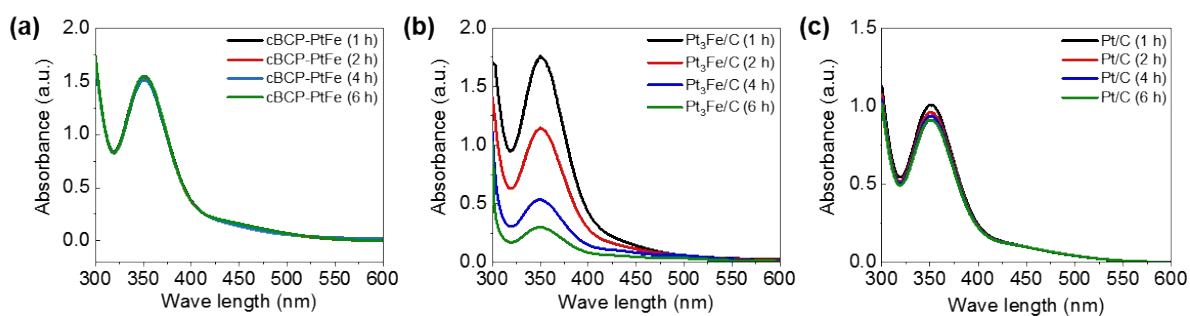


**Figure S24.** UV-Vis spectra for potassium hydrogen phthalate (KHP) decomposition test. The catalysts ((a) cBCP-PtFe (900 °C), (b) Pt<sub>3</sub>Fe/C, and (c) commercial Pt/C), H<sub>2</sub>O<sub>2</sub>, and KHP were stirred at 100 rpm and 80 °C for 1 h, 2 h, 4 h, and 6 h. When Fenton reaction occurs, the KHP peak at 350 nm would decrease because the leached Fe ions would have reactions with H<sub>2</sub>O<sub>2</sub>, generating OH· or OOH· radicals, which subsequently decompose KHP (Appl. Sci. 2019, 9, 23). The Pt<sub>3</sub>Fe/C were synthesized by depositing 108 mg of Pt(acac)<sub>2</sub> and 32 mg of Fe(acac)<sub>3</sub> on 200 mg of Vulcan carbon (XC 72R) using incipient impregnation method and reducing under H<sub>2</sub>/N<sub>2</sub> flow (20:180 sccm) at 500 °C for 2 h.

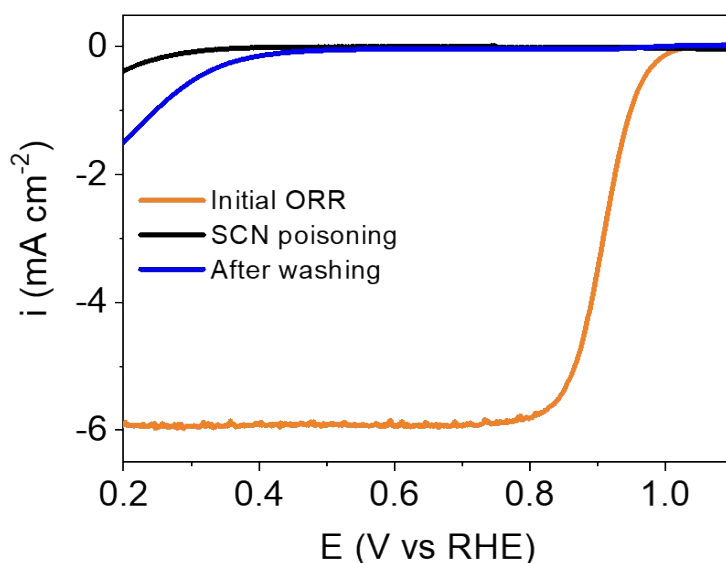


**Figure S25.** Selective poisoning on the PtFe nanoparticles without carbon shell. Oxygen reduction reaction (ORR) was performed in a half-cell setup for Pt<sub>1</sub>Fe<sub>1</sub>/C containing 20 wt% Pt. ORR curves for ‘SCN poisoning’ were obtained in 0.1 M HClO<sub>4</sub> including 30 mM KSCN. ORR curves for ‘after washing’ were obtained in pure 0.1 M HClO<sub>4</sub> after washing the SCN<sup>-</sup>-poisoned electrode in deionized water with 400 rpm for 1 h. The Pt<sub>1</sub>Fe<sub>1</sub>/C were synthesized by depositing 108 mg of Pt(acac)<sub>2</sub> and 98 mg of Fe(acac)<sub>3</sub> on 200 mg of Vulcan carbon (XC 72R) using incipient impregnation method and reducing under H<sub>2</sub>/N<sub>2</sub> flow (20:180 sccm) at 500 °C for 2 h.

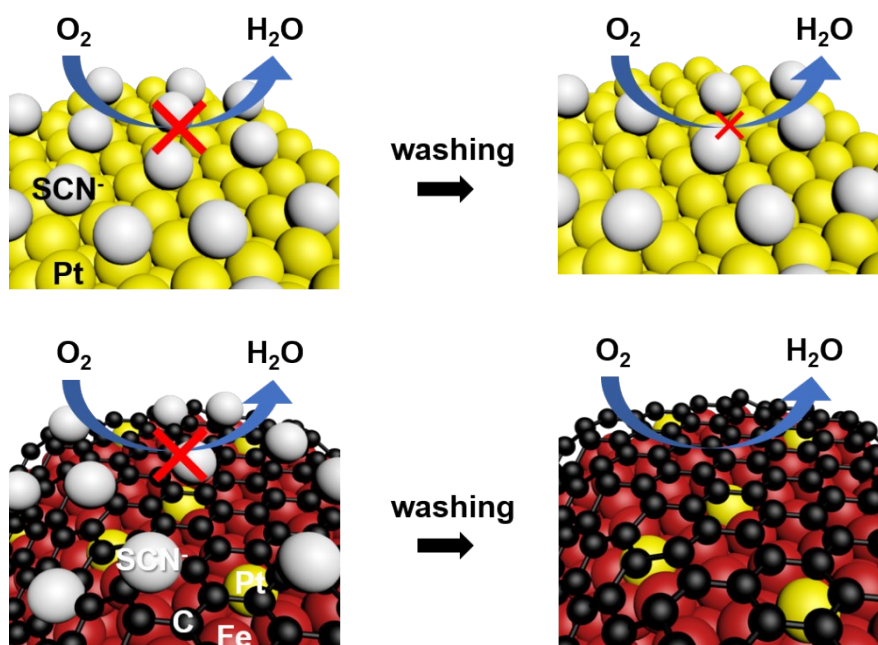


**Figure S26.** Schemes of ORR in the presence of  $\text{SCN}^-$ . The  $\text{SCN}^-$  remained on the commercial Pt/C after washing, hindering ORR. The  $\text{SCN}^-$  was easily removed on the cBCP-PtFe catalyst after washing, recovering the ORR activity.

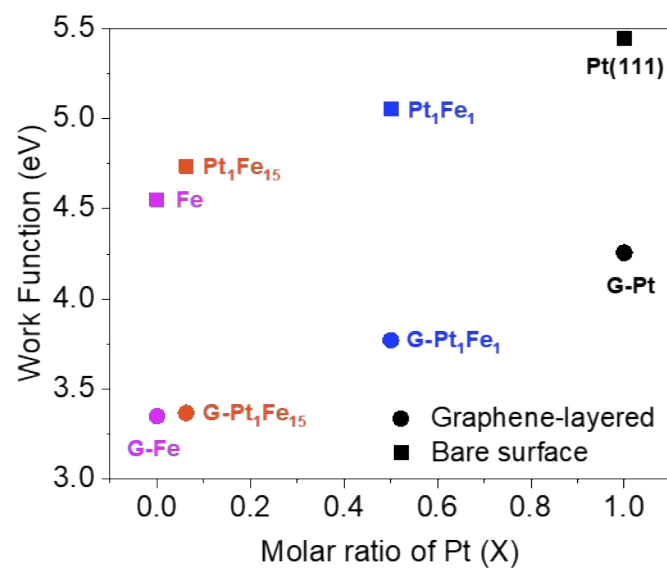


**Figure S27.** Work-function of graphene-layered or bare metal surface with various molar ratios of Pt, estimated by density functional theory calculations.